J. Non-Newtonian Fluid Mech. 157 (2009) 133–137

Contents lists available at ScienceDirect

Journal of Non-Newtonian Fluid Mechanics

journal homepage: www.elsevier.com/locate/jnnfm

Short communication

Electroosmotic flow of non-Newtonian fluid in microchannels

G.H. Tang*, X.F. Li, Y.L. He, W.Q. Tao

State Key laboratory of Multiphase Flow, School of Energy and Power Engineering, Xi'an Jiaotong University, Xi'an 710049, China

ARTICLE INFO

Article history:
Received 23 June 2008
Received in revised form 2 November 2008
Accepted 4 November 2008

Keywords:
Non-Newtonian
Microfluidics
Electroosmotic flow
Lattice Boltzmann method

ABSTRACT

Understanding electroosmotic flow of non-Newtonian fluid in microchannels is of both fundamental and practical significance for optimal design and operation of various microfluidic devices. A numerical study of electroosmotic flow in microchannels considering the non-Newtonian behavior has been carried out for the first time. One lattice Boltzmann equation is solved to obtain the electric potential distribution in the electrolyte, and another lattice Boltzmann equation which avoids the derivations of the velocity data to calculate the shear is applied to obtain the flow field for commonly used power-law non-Newtonian model. The simulation results show that the fluid rheological behavior is capable of changing the electroosmotic flow pattern significantly and the power-law exponent n plays an important role. For the shear thinning fluid of $n < 1$, the electrical double layer effect is confined to a smaller zone close to the wall surface and it is more inclined to develop into a plug-like flow whilst the shear thickening fluid of $n > 1$ is more difficult to grow into the plug-like flow compared to Newtonian fluid.

1. Introduction

Recent rapid development in micro-fabrication technology has enabled a variety of miniaturized fluidic systems consisting of micro ducts, valves, pumps, and nozzles. However, microfluidic devices are not simply scale-down version of conventional ones because fluid behaviors at microscale and macroscale are quite different. For example, electrokinetic and surface effects become important at microscale [1]. To optimize device design and operation, a better understanding of microscale fluidic transport phenomena is essential.

Because of no moving component, electroosmosis is often a preferred pumping method for microdevices over pressure-driven flow. Bulk movement of liquid in a microchannel can be achieved by applying an external electric field along the channel and important investigations have also been conducted [2,3]. However, to the authors' best knowledge, the existing electroosmotic flow studies are limited to Newtonian fluid. The flow behavior of non-Newtonian fluid is of high interest in many areas of science and technology. In practical applications for electroosmosis, such as sample collection, detection, mixing, and separation of various biological and chemical species on a chip integrated with fluidic pumps and valves, the fluid rheological behavior usually needs to be taken into account. Fundamental understanding of the non-Newtonian role in liquid transport through microchannels is important to correctly predict the performance and characteristics of microfluidic devices. In this paper, we numerically study the flow behavior of non-Newtonian fluids in the electroosmotic flow by using the lattice Boltzmann method (LBM). The recent development of the lattice Boltzmann method has provided an alternative simulation tool for computational fluid dynamics (CFD) [4]. The LBM differs from traditional numerical methods which solve the conventional macroscopic governing equations for the conserved fields such as flow field. The LBM tracks the evolution of the local distribution functions of the computational particles to describe the conserved fields. This makes the method extremely efficient for massively parallel computations especially in complicated systems including porous media, which are usually difficult for the existing continuum equation-based methods. In addition, the LBM originates from mesoscopic kinetic equations and intrinsically possesses some essential microscopic physics ingredients. This kinetic nature makes the LBM of great potential to capture the non-continuum effects including non-equilibrium and electrokinetic phenomena in microfluidic devices. Recently, the lattice Boltzmann model has been successfully applied in modeling a range of microfluidic electroosmotic applications [5–11]. In addition, the extension of the traditional LBM to non-Newtonian fluids has also recently received important attention [12–17].

The viscosity of the non-Newtonian fluid is related to the local rate of strain through the constitutive equation for the stress tensor. The kinetic essence of the LBM makes it capable of calculating the local components of the stress tensor in fluid flows without a need to estimate velocity gradients, compared to the Navier–Stokes solvers for which a need to get the derivatives of obtained velocity profiles is not avoidable. This feature makes the LBM retain

* Corresponding author.
E-mail address: ghtang@mail.xjtu.edu.cn (G.H. Tang).

0377-0257/$ – see front matter © 2008 Elsevier B.V. All rights reserved.
doi:10.1016/j.jnnfm.2008.11.002

second-order accuracy for shear-dependent non-Newtonian flow simulations [14].

The rest of the paper is organized as follows. In Section 2, we present the discrete Boltzmann equations for the velocity field of non-Newtonian fluid and for the electric potential distribution of electroosmotic flow, respectively. In Section 3, the presented LBM model is validated for a pressure-driven non-Newtonian flow, and then numerical simulations of electroosmotic flow for non-Newtonian fluid are demonstrated and discussed. A brief conclusion is given in Section 4.

2. Numerical methods

2.1. The lattice Boltzmann equation for non-Newtonian fluid flow field

The lattice Boltzmann method simulates transport phenomena by tracking the movement of molecule ensembles through the evolution of the distribution function, f. The discrete evolution equation with the Bhatnagar–Gross–Krook (BGK) collision approximation including an external force term, $\mathbf{F}$, is [18]

$$f_i(\mathbf{r}+\mathbf{c}_i\delta_t, t+\delta_t) = f_i(\mathbf{r},t) - \frac{\delta_t}{\tau_v}[f_i(\mathbf{r},t) - f_i^{eq}(\mathbf{r},t)] + \delta_t \frac{\mathbf{F}\cdot(\mathbf{c}_i-\mathbf{u})}{RT} f_i^{eq}(\mathbf{r},t), \quad (1)$$

where τ_v is the relaxation time and c_i is the particle discrete velocity. For a D2Q9 square lattice model, we have $c_0 = 0$, $c_i = (\cos[(i-1)\pi/2], \sin[(i-1)\pi/2])c$ for $i = 1, 2, 3, 4$ and $c_i = (\cos[(i-5)\pi/2+\pi/4], \sin[(i-5)\pi/2+\pi/4])\sqrt{2}c$ for $i = 5, 6, 7, 8$ where $c = \delta_x/\delta_t$ is the particle streaming speed (δ_x, δ_t are the lattice spacing and time step, respectively).

In Eq. (1), $f_i^{eq}(i = 0, 1, \ldots, 8)$ represents the equilibrium density distribution function, and for a D2Q9 lattice we have [19]

$$f_i^{eq} = \rho\omega_i\left[1 + \frac{3(\mathbf{c}_i\cdot\mathbf{u})}{c^2} + \frac{9(\mathbf{c}_i\cdot\mathbf{u})^2}{2c^4} - \frac{3(\mathbf{u}\cdot\mathbf{u})}{2c^2}\right], \quad (2)$$

where $\omega_0 = 4/9$, $\omega_i = 1/9$ for $i = 1, 2, 3, 4$ and $\omega_i = 1/36$ for $i = 5, 6, 7, 8$. The macroscopic variables such as mass density and momentum density can be obtained by summing over the distribution functions, $f_i(\mathbf{r},t)$:

$$\rho = \sum_i f_i \quad \text{and} \quad \rho\mathbf{u} = \sum_i f_i\mathbf{c}_i. \quad (3)$$

The relaxation time τ_v is related to the kinematic viscosity ν by

$$\tau_v = 3\nu\frac{\delta_t^2}{\delta_x^2} + 0.5\delta_t. \quad (4)$$

The stress tensor for an incompressible fluid with pressure p is given by

$$\sigma_{\alpha\beta} = -p\delta_{\alpha\beta} + \eta\left(\frac{\partial u_\alpha}{\partial x_\beta} + \frac{\partial u_\beta}{\partial x_\alpha}\right) = -p\delta_{\alpha\beta} + 2\eta S_{\alpha\beta}, \quad (5)$$

where η is the fluid dynamic viscosity, $\delta_{\alpha\beta}$ is the Kronecker delta, and $S_{\alpha\beta} = 1/2((\partial u_\alpha/\partial x_\beta) + (\partial u_\beta/\partial x_\alpha))$ is the shear strain rate tensor. $S_{\alpha\beta}$ can be calculated locally at each node in the LBM as [20]

$$S_{\alpha\beta} = -\frac{3}{2\rho c^2\tau_v}\sum_{i=0} f_i^{(1)}\mathbf{c}_{i\alpha}\mathbf{c}_{i\beta}, \quad (6)$$

where $f_i^{(1)}$ is the non-equilibrium part of the distribution function. In the commonly used power-law model for non-Newtonian fluid, the viscosity is given by

$$\eta = \eta_0\dot{\gamma}^{n-1} = \eta_0(S_{\alpha\beta}S_{\alpha\beta})^{(n-1)/2}, \quad (7)$$

where the shear rate-related $\dot{\gamma}$ is $\dot{\gamma} = \sqrt{S_{\alpha\beta}S_{\alpha\beta}}$ and the parameter n is the power-law exponent which determines the response of the fluid to changes in shear rate. The fluid is shear thinning for $n < 1$ and shear thickening for $n > 1$. The fluid recovers the Newtonian behavior with shear-independent viscosity η_0 for $n = 1$.

Coupling Eqs. (4), (6) and (7), together with $\eta = \rho\nu$, we have a shear-dependent relaxation time τ_v at each node in the lattice Boltzmann evolution Eq. (1).

Note that the quantity $f_i^{(1)}\mathbf{c}_{i\alpha}\mathbf{c}_{i\beta}$ in Eq. (6) is usually computed with second-order accuracy during the collision process in the LBM evolution. Therefore, the stress tensor components and the corresponding shear-dependent viscosity of non-Newtonian fluid can be obtained independent of the velocity fields, in contrast to most traditional CFD methods which estimate the stress tensor components from the obtained velocity field. This benefit without a need to get the derivatives of velocity profiles in computing the stress tensor and non-Newtonian viscosity is clear when dealing with flow in complex geometry of irregular cross-sections or flows characterized by large velocity gradients [21].

Using the Chapman–Enskog approximation, we can show that Eq. (1) recovers the Navier–Stokes equation:

$$\rho\left(\frac{\partial\mathbf{u}}{\partial t} + (\mathbf{u}\cdot\nabla)\mathbf{u}\right) = -\nabla p + \rho\nu\nabla^2\mathbf{u} + \rho\mathbf{F}. \quad (8)$$

For electrokinetic flows in dilute electrolyte solutions, the external force term can be simplified to

$$\rho\mathbf{F} = \rho_e\mathbf{E}_{ext} - \rho_e\nabla\Phi, \quad (9)$$

where ρ_e is the net charge density per unit volume at any point in the liquid, $\mathbf{E}_{ext}$ is the external electric field intensity and Φ is the electric potential caused by the ion movement in the solution. In general, the stream electric potential Φ, which could dominate the electro-viscosity effect in pressure-driven micro/nanochannel flow, can be neglected in pure electroosmotic flows in comparison with the applied external electricity [22].

2.2. The lattice Boltzmann equation for electric potential

From Eq. (9), it is known that the net charge density per unit volume, ρ_e, must be obtained before solving the velocity field. The relationship between the electric potential in the liquid, ψ, and the net charge density per unit volume, ρ_e, at any point in the liquid is described by the Poisson equation:

$$\nabla^2\psi = -\frac{\rho_e}{\varepsilon\varepsilon_0}, \quad (10)$$

where ε_0 is the permittivity of free space and ε is the relative dielectric constant of the solution. Assuming that the equilibrium Boltzmann distribution is applicable, the net charge density distribution can be expressed as the sum of all the ions in the solution:

$$\rho_e = \sum_\alpha z_\alpha e n_{\alpha,inf}\ \exp\left(-\frac{z_\alpha e\psi}{k_B T}\right), \quad (11)$$

where z_α and $n_{\alpha,inf}$ are the valence of type α ions and the bulk ionic concentration, respectively. The bulk ionic concentration, n_{inf}, can be expressed as the product of the ionic molar concentration, c_{inf}, and Avogadro's number, N_A. The constant, e, is the charge of a proton, k_B is Boltzmann's constant and T is the absolute temperature. Assuming a uniform dielectric constant and neglecting the fluctuation of the dielectric constant, we obtain the net charge density

distribution proportional to the concentration difference between the cations and anions [23]:

$$n_{\pm} = n_{inf} \exp\left(\mp\frac{ze\psi}{k_B T}\right), \tag{12}$$

$$\rho_e = ze(n_+ - n_-) = -2zen_{inf} \sinh\left(\frac{ze\psi}{k_B T}\right). \tag{13}$$

Substituting Eq. (11) into Eq. (10) yields the nonlinear Poisson–Boltzmann equation:

$$\nabla^2\psi + \frac{1}{\varepsilon\varepsilon_0}\sum_{\alpha} z_\alpha e n_{\alpha,inf} \exp\left(-\frac{z_\alpha e\psi}{k_B T}\right) = 0. \tag{14}$$

The following discrete lattice Boltzmann evolution equation for the electric potential has been derived by [9,24]

$$g_i(\mathbf{r} + \mathbf{c}_i\delta_t, t + \delta_t) = g_i(\mathbf{r}, t) - \frac{\delta_t}{\tau_g}[g_i(\mathbf{r}, t) - g_i^{eq}(\mathbf{r}, t)] + \frac{(\tau_g - 0.5\delta_t)\delta_t\omega_i}{\tau_g} \times \left(\frac{1}{\varepsilon\varepsilon_0}\sum_{\alpha} z_\alpha e n_{\alpha,inf} \exp\left(-\frac{z_\alpha e\psi}{k_B T}\right)\right), \tag{15}$$

where g is the distribution function and g^{eq} is the corresponding equilibrium distribution function on a D2Q9 lattice, with $g_0^{eq} = 0$, $g_{1,2,3,4}^{eq} = \psi/6$, and $g_{5,6,7,8}^{eq} = \psi/12$. The potential diffusivity, χ, which is equal to unity in the simulations, is defined as

$$\chi = \frac{2(\tau_g - 0.5\delta_t)}{3}\frac{\delta_x^2}{\delta_t^2}. \tag{16}$$

The macroscopic electric potential in the liquid is calculated from

$$\psi = \sum_i g_i + \frac{\delta_t}{2}\sum_i \left(\frac{1}{\varepsilon\varepsilon_0}\sum_{\alpha} z_\alpha e n_{\alpha,inf} \exp\left(-\frac{z_\alpha e\psi}{k_B T}\right)\right)\omega_i. \tag{17}$$

2.3. The boundary conditions for the lattice Boltzmann equations

Due to its kinetic nature and essential character of microscopic physics, the lattice Boltzmann method is of good capability for handling more general boundary conditions. To solve the lattice Boltzmann equation for the electric potential, the zeta potentials at the upper and lower walls are fixed and the Dirichlet boundary conditions are employed [25]. The periodic boundary conditions are applied for the electric potentials at the channel inlet and outlet. For the velocity field, the non-slip boundary conditions at the upper and lower walls proposed by Zou and He [26] are adopted, and the periodic boundary conditions are applied again at the channel inlet and outlet.

3. Results and discussion

3.1. Pressure-driven channel flow

To validate the present lattice Boltzmann model for non-Newtonian fluid, a pressure-driven flow between two parallel plates is considered. The lower and upper non-slip walls are defined by $y = 0$ and H. A uniform pressure gradient dp/dx is applied along the streamwise direction as the external force. For the power-law fluid, an analytical solution for streamwise velocity across the channel is given by [27]

$$\frac{u(y)}{u_m} = \frac{2n+1}{n+1}\left[1 - \left(\frac{|2y - H|}{H}\right)^{(n+1)/n}\right], \tag{18}$$

where u_m is the mean velocity across the channel.

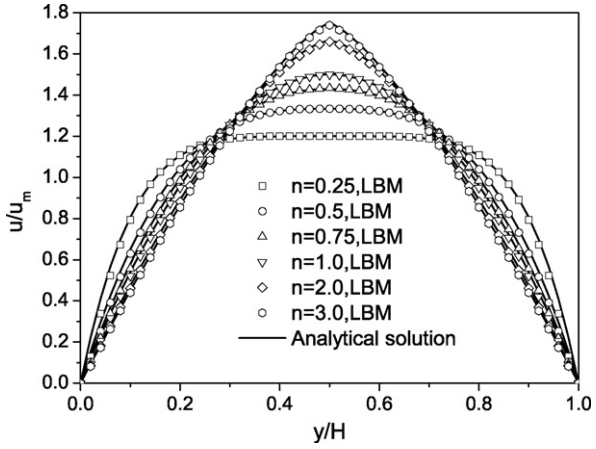

Fig. 1. Comparisons between the LBM results and the analytical solutions in the pressure-driven non-Newtonian flow.

Simulations were run for $n = 0.25$, 0.5, 0.75, 1.0, 2.0 and 3.0 in order to test the LBM accuracy for a range of non-Newtonian behaviors. Fig. 1 shows the LBM results (symbols) compared to normalized analytical velocity profiles (solid lines) over the range of n parameter values. The agreement with the analytical solutions is quite good. It can be seen that the LBM predicts the correct velocity profiles for both shear thinning ($n < 1$) and shear thickening ($n > 1$) flows, as well as Newtonian flows ($n = 1$). Compared to Newtonian flows of $n = 1$ for $n < 1$ we can see a general flattening of the velocity profile, with more flat velocity profiles corresponding to lower n. In contrast, the velocity profiles for $n = 2.0$ and 3.0 show greater curvature around the center peak velocity. The profile presents significant sharp-tip at $n = 3.0$ around the center peak velocity as shown in Fig. 1. The ratio of the center peak velocity to the channel mean velocity increases as the index n increases.

3.2. Electroosmotic channel flow

A simple electroosmotic flow between two parallel plates is considered. The external force is applied in the flow as shown in Eq. (9). In the simulation, we choose $\varepsilon\varepsilon_0 = 7.79 \times 10^{-10}$ C^2/(J m), $T = 273$ K, $e = 1.6 \times 10^{-19}$ C, $N_A = 6.02 \times 10^{23}$ mol^{-1}, $k_B = 1.38 \times 10^{-23}$ J/K, $\rho = 1000$ kg/m^3, $z = 1$, $\nu_0 = 1.789 \times 10^{-6}$ m^2/s, the surface zeta potential of $\zeta = -100$ mV, and the externally applied electric field intensity of $E = 500$ V/m.

Fig. 2(a) and (b) present the normalized streamwise velocity profile across the channel for $c_{inf} = 10^{-7}$ mol/l and 10^{-4} mol/l, respectively. We can see that for the Newtonian fluid of $n = 1$, the velocity profile is parabolic at lower ionic concentration, which resembles a typical pressure-driven flow. However, as the bulk ionic concentration increases, the velocity profile transits from parabolic to plug-like. The velocity profiles for non-Newtonian flow of $n = 2.0$ and 3.0 show curvature and sharp-like around the center peak velocity whilst the case of $n = 0.5$ presents typical plug flow for the both shown ionic concentrations. The velocity profiles for all the values of n exhibit more flattening at $c_{inf} = 10^{-4}$ mol/l compared to $c_{inf} = 10^{-7}$ mol/l. These different flow profiles are caused by variations in the Debye length, λ_D, which is used to describe the characteristic thickness of the electric double layer (EDL):

$$\lambda_D = \sqrt{\frac{\varepsilon\varepsilon_0 k_B T}{2N_A c_{inf} e^2 z^2}}. \tag{19}$$

The calculated Debye length for $c_{inf} = 10^{-4}$ mol/l is 0.02915 μm, compared to 1.01 μm for $c_{inf} = 10^{-7}$ mol/l. Inside the EDL, the velocity profile is not plug-like and changes drastically. In electroosmotic flow, a driving force generated by the interaction of the EDL with

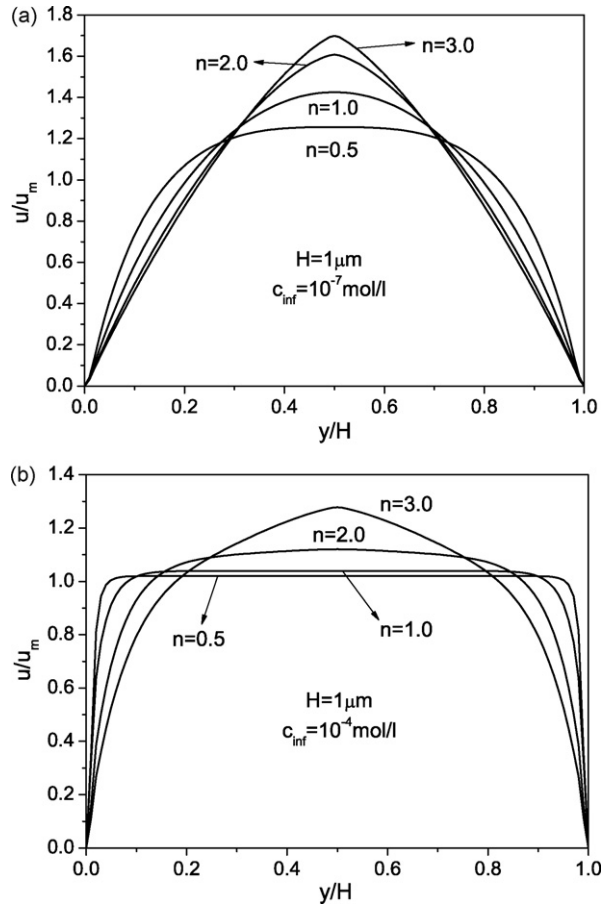

Fig. 2. Normalized velocity profiles for various power-law exponents n at two different ionic concentrations in the electroosmotic flow. (a) $c_{inf} = 10^{-7}$ mol/l and (b) $c_{inf} = 10^{-4}$ mol/l.

the external electric field exists inside the EDL in the vicinity of the wall surfaces. The fluid movement outside the EDL is dragged by the fluid within the EDL. Consequently, the electroosmotic flow is capable of sustaining. However, for the pressure-driven flow, the entire cross section of the channel experiences the pressure-driven force. As noted in our previous work [24], the velocity profile for Newtonian flow behaves plug-like when the ratio of the channel height to the Debye length is larger than about 10. It can also be observed from Fig. 3(a), in which velocity profiles normalized by the channel center velocity u_c are presented for three channel heights at $\lambda_D = 0.02915\,\mu m$. The velocity profiles for channel heights $H = 0.1\,\mu m$ and $0.2\,\mu m$ are still parabolic whilst the profile transits to be typically plug-like at $H = 0.4\,\mu m$. We believe that this change be caused by the overlapping or closely overlapping of the electrical double layers, since the Debye length measures the range of electrostatic influence of the single ions. Fig. 3(b) shows the normalized velocity profiles for non-Newtonian fluid of $n = 1.5$ at $\lambda_D = 0.02915\,\mu m$. We can see that the profiles are not plug-like until $H = 1.0\,\mu m$, which is quite larger than 10 times of the Debye length. However, for the case of $n = 0.5$, the normalized velocity profile is plug-like even at $H = 0.05\,\mu m$ and all the profiles presented in Fig. 3(c) are almost identical.

As we know, generally, the benefit of plug-like velocity profile facilitates electroosmotic flow of significant applications in the microfluidic fields including micro pump, mixing, and fluid motion-control. However, our investigation shows that the velocity profile is significantly dependent on the fluid rheological behavior. The shear thickening fluid is more difficult to grow into a plug-like flow than Newtonian fluid. In contrast, for the shear thinning fluid, the

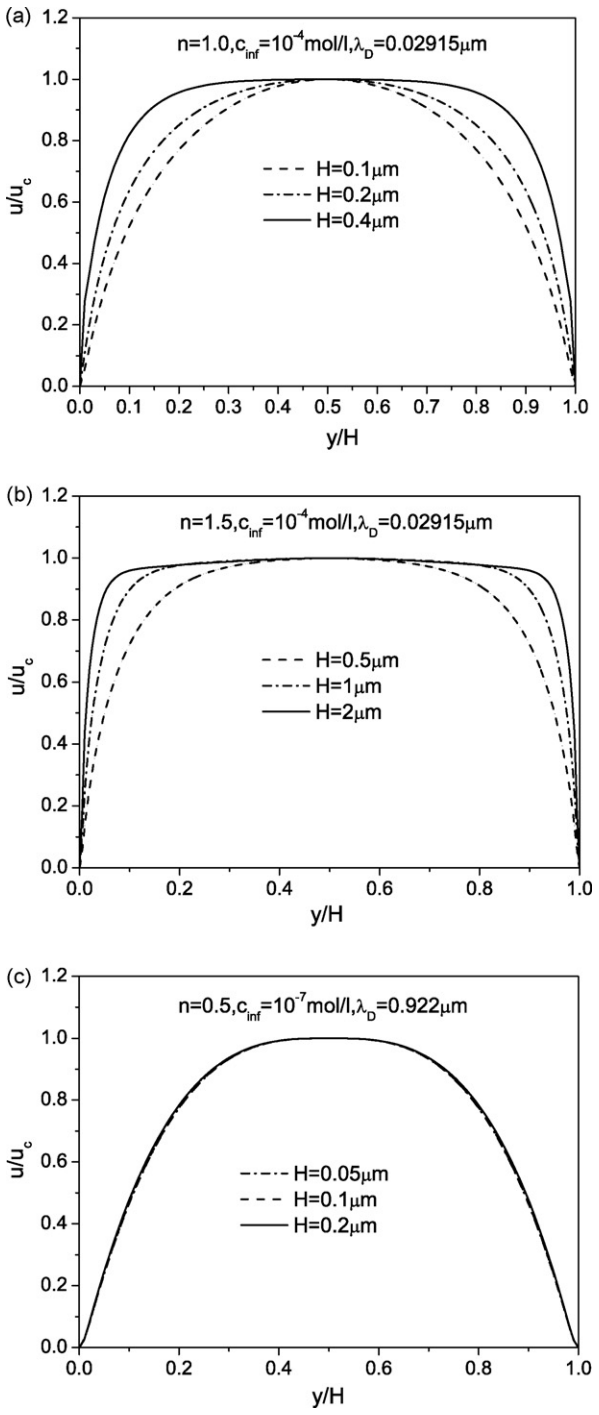

Fig. 3. Normalized velocity profiles for various channel heights at different ionic concentrations and power-law exponents n in the electroosmotic flow. (a) $n = 1.0$, $c_{inf} = 10^{-4}$ mol/l. (b) $n = 1.5$, $c_{inf} = 10^{-4}$ mol/l. (c) $n = 0.5$, $c_{inf} = 10^{-7}$ mol/l.

electric double layer effect is confined to a smaller zone close to the wall surface and it is more inclined to develop into the plug-like flow.

4. Conclusions

Motivated by the growing interest in electroosmosis as a no-moving-component method to pump, mix, and control fluid motion in microfluidic devices, we have numerically studied the non-Newtonian fluid for electroosmotic flow in microchannels for the first time. We have applied the lattice Boltzmann methodology

to describe the electric potential distribution in the electrolyte and the flow field. The presented second-order accurate LBM for shear-dependent non-Newtonian flow field avoids time consuming derivations of the velocity data to calculate the shear. We have focused our work on power-law fluids with various exponents n, though the method is sufficiently general to other stress–shear rate relationships.

It is found that the fluid rheological character is capable of changing the electroosmotic flow pattern significantly and the power-law exponent n plays an important role. For the Newtonian flow, the velocity profile presents plug-like when the ratio of channel height to the Debye length is larger than about 10. However, the critical value changes significantly for the non-Newtonian flow. For the shear thickening fluid, the critical ratio of the channel height to the Debye length is much larger than 10 whilst the critical ratio is much smaller than 10 for shear thinning fluid. The shear thickening fluid is more difficult to grow into a plug-like flow. In contrast, for the shear thinning fluid, the electrical double layer effect is confined to a smaller zone close to the wall surface. It is more inclined to develop into a plug-like flow and the velocity profile exhibits more flattening across most of the channel. The present study shows that the non-Newtonian behavior of the transport fluid must be taken into account in the practical electroosmotic microfluidic applications.

Acknowledgments

This work was supported by the National Natural Science Foundation of China (No. 50776067) and by the Program for New Century Excellent Talents in University of China (NCET-07-0676).

References

[1] G. Karniadakis, A. Beskok, N. Aluru, Microflows and Nanoflows Fundamentals and Simulation, Springer, New York, 2004.
[2] P. Dutta, Numerical modeling of electroosmotically driven flows in complex micro-geometries, Ph. D. thesis, Texas A&M University, College Station, 2001.
[3] L.Q. Ren, D.Q. Li, Electroosmotic flow in heterogeneous microchannels, J. Colloid Interface Sci. 243 (2001) 255.
[4] S. Chen, G.D. Doolen, Lattice Boltzmann method for fluid flows, Annu. Rev. Fluid. Mech. 30 (1998) 329.
[5] B.M. Li, D.Y. Kwok, Lattice Boltzmann model of microfluidics in the presence of external forces, J. Colloid Interface Sci. 263 (2003) 144.
[6] B.M. Li, D.Y. Kwok, Electrokinetic microfluidic phenomena by a lattice Boltzmann model using a modified Poisson-Boltzmann equation with an excluded volume effect, J. Chem. Phys. 120 (2004) 947.
[7] F.Z. Tian, D.Y. Kwok, On the surface conductance, flow rate, and current continuities of microfluidics with nonuniform surface potentials, Langmuir 21 (2005) 2192.
[8] J.K. Wang, M. Wang, Z.X. Li, Lattice Poisson–Boltzmann simulations of electro-osmotic flows in microchannels, J. Colloid Interface Sci. 296 (2006) 729.
[9] S. Melchionna, S. Succi, Electrorheology in nanopores via lattice Boltzmann simulation, J. Chem. Phys. 120 (2004) 4492.
[10] Z.L. Guo, T.S. Zhao, Y. Shi, A lattice Boltzmann algorithm for electro-osmotic flows in microfluidic devices, J. Chem. Phys. 122 (2005) 144907.
[11] Z.H. Chai, Z.L. Guo, B.C. Shi, Study of electro-osmotic flows in microchannels packed with variable porosity media via lattice Boltzmann method, J. Appl. Phys. 101 (2007) 104913.
[12] E.S. Boek, J. Chiny, P.V. Coveney, Lattice Boltzmann simulations of the flow of non-Newtonian fluids in porous media, Int. J. Mod. Phys. B 17 (2003) 99.
[13] S. Gabbanelli, G. Drazer, J. Koplik, Lattice Boltzmann method for non-Newtonian (power-law) fluids, Phys. Rev. E 72 (2005) 046312.
[14] J. Boyd, J. Buick, S. Green, A second-order accurate lattice Boltzmann non-Newtonian flow model, J. Phys. A 39 (2006) 1424.
[15] S.P. Sullivan, L.F. Gladden, M.L. Johns, Simulation of power-law fluid flow through porous media using lattice Boltzmann techniques, J. Non-Newtonian Fluid Mech. 133 (2006) 91.
[16] S.P. Sullivan, L.F. Gladden, M.L. Johns, L.F. Gladden, Verification of shear-thinning LB simulations in complex geometries, J. Non-Newtonian Fluid Mech. 143 (2007) 59.
[17] C.H. Wang, J.R. Ho, Lattice Boltzmann modeling of Bingham plastics, Physica A 387 (2008) 4740.
[18] X.Y. He, L.S. Luo, Theory of the lattice Boltzmann method: from the Boltzmann equation to the lattice Boltzmann equation, Phys. Rev. E 56 (1997) 6811.
[19] Y.H. Qian, D. d'Humieres, P. Lallemand, Lattice BGK models for Navier–Stokes equation, Europhys. Lett. 17 (1992) 479.
[20] A.M. Artoli, Mesoscopic Computational Haemodynamics, Ponsen & Looijen, Wageningen, 2003.
[21] A.M. Artoli, A.G. Hoekstra, P.M.A. Sloot, Optimizing lattice Boltzmann simulations for unsteady flows, Comput. Fluids 35 (2006) 227.
[22] G.H. Tang, Z. Li, Y.L. He, C.Y. Zhao, W.Q. Tao, Experimental observations and lattice Boltzmann method study of the electroviscous effect for liquid flow in microchannels, J. Micromech. Microeng. 17 (2007) 539.
[23] C.L. Ren, D.Q. Li, Improved understanding of the effect of electrical double layer on pressure-driven flow in microchannels, Anal. Chim. Acta 531 (2005) 15.
[24] G.H. Tang, Z. Li, J.K. Wang, Y.L. He, W.Q. Tao, Electroosmotic flow and mixing in microchannels with the lattice Boltzmann method, J. Appl. Phys. 100 (2006) 094908.
[25] G.H. Tang, W.Q. Tao, Y.L. He, Thermal boundary condition for the thermal lattice Boltzmann equation, Phys. Rev. E 72 (2005) 016703.
[26] Q. Zou, X.Y. He, On pressure and velocity boundary conditions for the lattice Boltzmann BGK model, Phys. Fluids 9 (1997) 1591.
[27] N. Rakotomalala, D. Salin, P. Watzky, Simulations of viscous flows of complex fluids with a Bhatnagar, Gross, and Krook lattice gas, Phys. Fluids 8 (1996) 3200.